

REPLICA: Enhanced Feature Pyramid Network by Local Image Translation and Conjunct Attention for High-Resolution Breast Tumor Detection

Yifan Zhang, Haoyu Dong, Nicolas Konz, Hanxue Gu, Maciej A. Mazurowski
Duke University

{yifan.zhang507, haoyu.dong151, nicholas.konz, hanxue.gu, maciej.mazurowski}@duke.edu

Abstract

We introduce an improvement to the feature pyramid network of standard object detection models. We call our method enhanced feature Pyramid network by Local Image translation and Conjunct Attention, or REPLICA. REPLICA improves object detection performance by simultaneously (1) generating realistic but fake images with simulated objects to mitigate the data-hungry problem of the attention mechanism, and (2) advancing the detection model architecture through a novel modification of attention on image feature patches. Specifically, we use a convolutional autoencoder as a generator to create new images by injecting objects into images via local interpolation and reconstruction of their features extracted in hidden layers. Then due to the larger number of simulated images, we use a visual transformer to enhance outputs of each ResNet layer that serve as inputs to a feature pyramid network. We apply our methodology to the problem of detecting lesions in Digital Breast Tomosynthesis scans (DBT), a high-resolution medical imaging modality crucial in breast cancer screening. We demonstrate qualitatively and quantitatively that REPLICA can improve the accuracy of tumor detection using our enhanced standard object detection framework via experimental results.

1. Introduction

Object detection (OD) is one of the most important tasks in computer vision [37]. Its application is diverse, ranging from detecting dynamic objects in crowd-counting, self-driving cars and video surveillance, to static objects in face recognition and industrial anomaly detection.

Having a reliable model for object detection is essential. Attention mechanisms [47] have already shown great success when applied to computer vision, such as the use of pixel-wise, pair-wise and patch-wise self-attention for image recognition [21, 38]. Attention-based neural networks generally out-perform traditional convolutional neural net-

works (CNNs) on large-scale detection tasks, as the former allow for the scalable perception of an entire image, while the inefficiency of CNN receptive fields only allow for the perception of local image patches. The Visual Transformer (ViT) [16] and Swin Transformer [34] are two examples of such attention-based computer vision backbones. Such methods can logically also benefit the task of object detection, allowing for the creation of more reliable tumor detection frameworks.

Since the success of attention [47], this mechanism has been applied to OD, and has advanced the performance of OD, including OD with pyramid constrained self-attention [19], OD with dynamic attention [13] and OD with spatiotemporal attention [52]. More recently, given the success of transformers on images (ViT), Swin has been proposed as the state-of-the-art (SOTA) backbone for attention.

Despite the success of attention, we note that it is difficult to directly apply to medical images because most attention-based methods rely on the assumption that the task domain is of natural images, which usually have diverse object classes, are plentiful, and are of relatively moderate resolution. Specifically, we list the following distinct properties of medical images that prevent the success of attention: **High-resolution of medical images.** Applying spatial attention directly to medical images is impractical on modern hardware, as the size of medical images is generally considerably larger than natural images. Most medical images used for tumor detection have a resolution of more than 2560×1920 [5], while the resolution of natural images only contains 3 – 5% pixels when compared to medical images [11, 14, 29, 35], making tumor detection using such models unrealistic in terms of computational complexity and resource availability.

Label & annotation scarcity. On the other side, there are usually not enough labelled data and annotated regions in medical scenarios to robustly train an attention mechanism. In a typical tumor detection dataset, healthy scans outnumber cancerous scans by a factor of about 200, due to the natural rarity of such cases in a randomly sampled screening population [36]. Furthermore, within scans that include

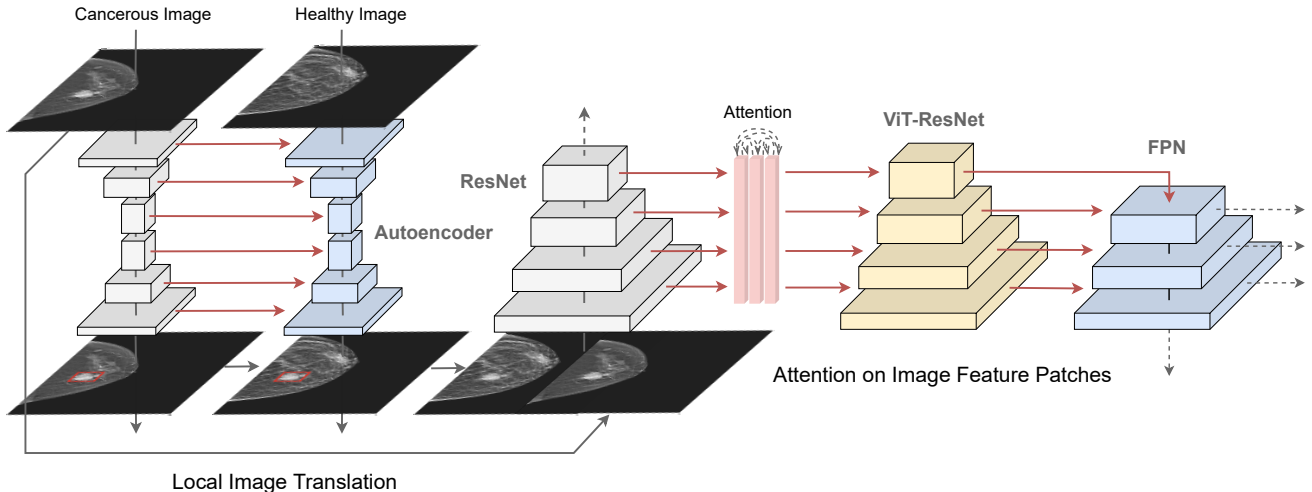


Figure 1. REPLICA’s entire model architecture. It has two modules: on the left is the module for local image translation in 3.1, and on the right is the feature pyramid network with multi self-attention on image feature patches of ResNet outputs in 3.2.

tumors, the size of the tumor can often be less than 1/40 of the size of the entire image [5]. As a result, traditional machine learning methods can be very difficult to implement successfully for this domain.

To address the first problem, we adopt the attention method first proposed by ViT, instead of applying full-size images directly to the model. Specifically, we replace the FPN module, which naively sums the features from different layers, with an attention-based integration. To address the second problem, we train a local image translation model to augment existing tumor-labelled data and generate fake tumor images that are interpolated and reconstructed by their features extracted in hidden layers of the generator to expand the receptive field of visual transformer. The entire model structure is shown in Fig.1. To the best of our knowledge, REPLICA is the first work that addresses these major issues in tumor detection while also employing the attention mechanism on patches of hidden features of an image for enhancing the feature pyramid network (FPN) [28]. Compared to the baseline Faster-RCNN [40] model, our model achieves 50.4 in AP50, which outperforms the baseline by at least 13.1%. We also conduct ablation studies to prove the effectiveness of each proposed modification.

In summary, our contributions are as follows:

1. We generate realistic but fake images with tumors to mitigate the data-hungry problem in attention-based object detection model architecture for tumor detection.
2. We advance the detection model architecture through a novel backbone of attention on image feature patches on ResNet outputs that serve as inputs to FPN to improve the performance of tumor detection.

2. Related Works

Image-to-Image Translation. The objective of image-to-image translation is to discover a correspondence between an input and output image. Such models are divided into two primary classes: generative adversarial networks (GANs) based models [18], and *inversion* based ones. Pix2Pix [23] and CycleGAN [57] are two common paired and unpaired GAN-based translation models, respectively. Due to the scarcity of natural pairings of pictures for paired image translation, the majority of subsequent research focuses on *unpaired* data for image translation, such as the fields of multi-domain translation and image fidelity [9, 30, 31]. Recent research has also concentrated on representation disentanglement in terms of style, texture, and form [41, 53, 54], as well as multi-modal learning to keep cross-modal information or to produce diverse results during translation [2, 12, 22, 33, 58]. Finally, classifier-based inversion is a type of method where the objective is to construct a picture by modifying the hidden features of a trained classifier [42]. IMAGINE [48], one of the more recent of such models, incorporates a feature inversion technique that allows for the creation of a picture with a merged style from a single image.

For our scenario, the scarcity and complexity of tumor image data makes learning useful representations of tumors challenging and impracticable. Instead of generating new tumor pictures with trained GAN-styled models, we use an AutoEncoder [24] to reconstruct tumor images using heuristically selected and paired normal images in order to circumvent methods such as distribution learning and generalization that have higher dataset size requirements. To modify hidden features during reconstruction in order to realistically translate tumor objects into generated pictures,

we also use *progressive translation*, which is inspired by model inversion ideas.

Attention and Visual Transformer. Self-attention mechanisms, which first appeared as methods for dependency-modeling within sequences in natural language processing (NLP) tasks [47], have parameter-independent receptive field scaling and content-dependent interactions, making them effective for computer vision research. They have subsequently been integrated into a number of downstream vision tasks, including image classification, object detection, and segmentation [3, 43, 46]. Meanwhile, given the computationally cost of conducting spatial attention, researchers have turned to *attention on image patches* in vision tasks to enhance training efficiency [16]. Some recent works have focused on detecting saliency and context in visual recognition using ViT [26, 32].

Object Detection. Object detection is a central component of visual analysis and comprehension [55]. Besides general architectural innovations in multi-scale interaction, generalization and attention with CNNs [6, 7, 44], there are two mainstream research directions of object detection. These include two stage region proposal-based object detection frameworks [4, 40, 56] and one stage regression-based frameworks [17, 39]. Faster R-CNN [40] and YOLO [17] some are the most common models for these two approaches, respectively. Object detection and segmentation frameworks include Detectron2 [50] and MMDetection [8], which possess capabilities of data augmentation, bounding boxes rotation and computational efficiency.

Inspired by various attention models in vision tasks and feature pyramid networks in object detection, we propose a method that allows us to connect the attention mechanism of ViT on image feature patches to the ResNet [20] backbone of a FPN and find a balance between computational complexity and model performance improvement through the attention mechanism on patches of hidden features of an image. The coupling of our object detection model and data augmentation allows us to mitigate the data-hungry problem of attention mechanism and attain higher performance in the task of tumor detection.

3. Proposed Method

In this section, we present the following sequentially. (1) Our local image translation module that uses a convolutional autoencoder to interpolate and reconstruct the features of normal and tumor images in hidden layers to get realistic but fake tumor images. (2) Our feature pyramid network with attention on the image feature patches of ResNet outputs. (3) The integrated REPLICA model that utilizes these generated tumor images to improve the performance of our attention-guided feature pyramid network.

3.1. Progressive Translation by Image Reconstruction

We consider a basic convolutional autoencoder model as our baseline model. We perform local translation by interpolating and reconstructing the features of both tumor and normal images in hidden layers of the autoencoder, and crop the region of tumors to the same positions in paired normal images. The spatial information within hidden layers of such a model can provide useful details of specific areas in the original input image [1], which is helpful for local translation. Additionally, by avoiding the usage of a generative model (*e.g.* a GAN) for distribution learning, this model is made effective by using overfitting to maintain the original information of the images as much as possible, and the generated images will preserve the high quality of the input images. The entire procedure is depicted in Fig. 2.

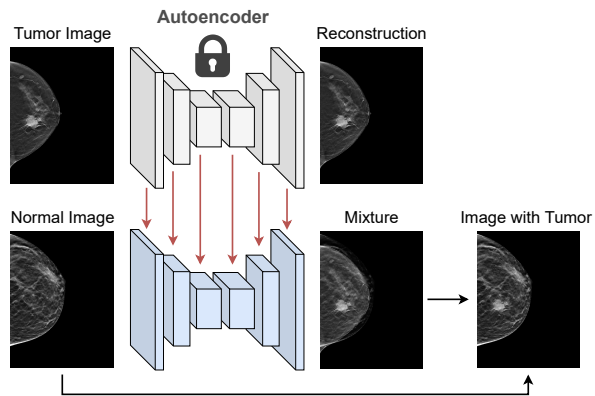


Figure 2. The local image translation framework of our model. The lock icon represents an autoencoder image reconstruction model that has been pretrained and overfitted with a convolutional autoencoder. Data flow and intra-model computation are shown by dark gray arrows, whereas inter-model computation is denoted by red arrows.

The basic idea behind autoencoders for image reconstruction is to train convolutional encoder and decoder neural networks to convert an image to a lower-dimensional feature representation, and then back to the same image, respectively [25]. The autoencoder training objective can be written as

$$(e^*, d^*) = \arg \min_{e, d} L(x, d(e(x))), \quad (1)$$

where e^* and d^* denote the optimal encoder and decoder, x and $d(e(x))$ are the input image and the reconstructed image, and $L(x, d(e(x)))$ defines the reconstruction error between them. We use an L_1 reconstruction loss of

$$L_{ae} = \|x - d(e(x))\|_1. \quad (2)$$

The first step for the image reconstruction model is to

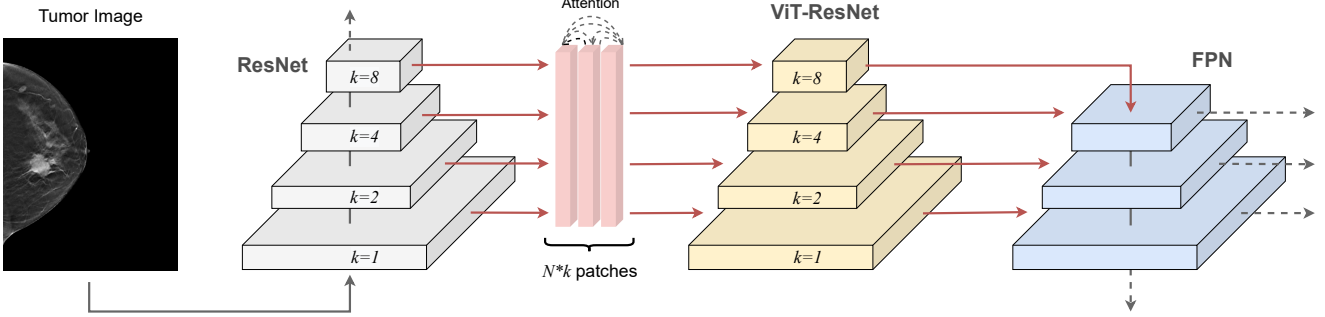


Figure 3. The framework of conjunct attention in our model. There are four hidden levels in the ResNet50 backbone, each containing 256, 512, 1024, and 2048 channels. Each convolutional layer reduces the size of the image by half. The number of image feature patches in each layer is denoted by N . If we set the patch size as (5, 4) and the input size to the first layer of ResNet is (640, 512), N for each hidden layer will be 64^2 , 32^2 , 16^2 , and 8^2 , respectively.

obtain paired normal and tumor images through a novel-designed heuristic image-matching rule, which ensures that a tumor is always within the outline or a normal image. Furthermore, to ensure the reconstruction quality, we select a balanced number of healthy and tumor scans, which serves as the input to the generation model.

We further propose to overfit the model with the input data, *i.e.*, obtain $L_{ae} \simeq 0$. While this seems counter-productive to machine learning standards, we argue that such a method enables the model to capture most textures, shapes and color information that is crucial for the reconstruction process. After AE converges, we input a pair of normal and tumor images (\mathbf{x}, \mathbf{y}) and interpolate between the two representations as follows:

$$g(\mathbf{x}) = (1 - \lambda_k) \cdot g(\mathbf{x}) + \lambda_k \cdot g(\mathbf{y}), \quad (3)$$

where $g(\mathbf{x})$ and $g(\mathbf{y})$ denote the feature maps of the translated healthy image and cancerous image, respectively, obtained from the hidden layers of the convolutional autoencoder, k denotes the k_{th} hidden layer of the reconstruction model, k should be related to $g(\mathbf{x})$ and λ_k is the hidden feature ratio of the tumor image that will be interpolated with those of the normal image. To enable progressive content translation from the cancerous image to the healthy image, λ_k should increase continuously with k , but should be less than 1, for both encoder and decoder layers.

In the final step of translation we merge the created mixed image with the paired normal image by cropping the content within the bounding box annotation of the tumor provided with the cancerous scan. Following this we use several pixel-level processing techniques, including marginal transition, boundary division, and cropping, to obtain a higher-quality image, which are attached in appendix.

3.2. Attention Guided Feature Pyramid

We propose a new ViT backbone for coupling with the feature pyramid network in order to improve detection per-

formance. In our pipeline, raw images are fed into a ResNet50 to generate feature maps corresponding to the activation map of each hidden layer. Because spatial attention can significantly improve the connections between pixels, before feeding these out-puts into the next Feature Pyramid Network (FPN) [28] that uses multi-scale pyramidal hierarchy to construct feature pyramids for Region Proposal Network (RPN) and Region of Interest (RoI) pooling [40], we use attention on image feature patches of the outputs of ResNet to improve the hidden representations of each inputs to FPN.

The entire procedure of our ViT-ResNet is shown in Fig.3. It is divided into three parts: feature map transformation, attention on image feature patches, and feature map reconstruction. Each patch of feature map in the ResNet outputs will be subjected to the following transformation in the first section:

$$\mathbf{z} = [\mathbf{x}_p^1 \mathbf{E}; \mathbf{x}_p^2 \mathbf{E}; \dots; \mathbf{x}_p^N \mathbf{E}]. \quad (4)$$

Since the output of ResNet follows a pyramid structure, with the increment in hidden dimension and stride over spatial dimension, we use divisible numbers of the spatial size of the last-layer representation as the patch size, which is (5, 4). Then, all shallow layers are first resized along hidden dimension to match the depth information, *i.e.*, $(256 \times 2, h \times w) \rightarrow (256, (2h \times w))$.

As with BERT [15] and ViT, we append a learnable positional embedding E_{pos} to assist the network in remembering the locations of individual patches, as

$$\mathbf{z} = \mathbf{z} + E_{pos}. \quad (5)$$

Due to the fact that each ResNet feature map has a numbers of channels and patches, we utilize a positional embedding with a maximum length of $N \cdot \max(k)$ in our proposed model, where $\max(k) = 8$. Following that, the ViT-ResNet module's final output is computed as

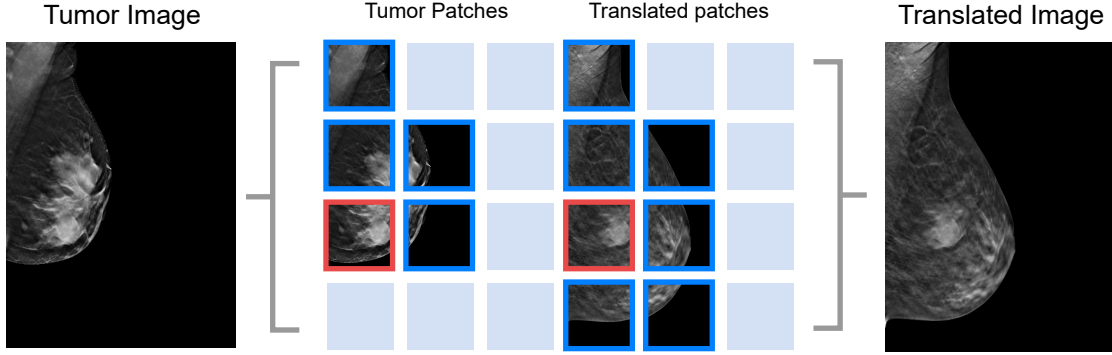


Figure 4. The integrated framework is shown in this diagram. The red boxes indicate patches containing real or translated tumor, while the blue boxes provide relevant background information. The original tumor patch can only have 4 reference patches in the background, whereas the number increases to 9 when a translated normal image is provided.

$$z' = MSA(LN(z) + z), \quad (6)$$

where MSA denotes multi self-attention, and LN is layer-wise normalization [47]. In contrast to ViT’s classification task design, we retain multi self-attention (MSA), but remove the multilayer perceptron (MLP) and classification token, and keep the final dimension fixed to the original dimension of the patch to generate the input of the subsequent FPN.

3.3. Integrated Model Details

By combining the local image translation and the attention-guided feature pyramid network, REPLICa mitigates the data-hungry problem in attention with a larger number of generated realistic but fake cancerous images, and fully exploits the hidden information contained in each tumor image by applying attention on image feature patches.

Because of the abundance of source images in common computer vision tasks, researchers can simply employ various advanced ViT architectures, such as DeiT [45] and PVT [49], that partition images into distillation embeddings or feature pyramids to boost model performance [10, 27]. However, because there are only a few tumor images in our case, it is almost impossible for the attention mechanism to learn sufficient background information for the object to be detected.

Given the constraint from fully attention-based model, we first replace only a component of the models with ViT. This is further improved by local image translation that introduces extra fake label images. We have found that local image translation is an effective method for introducing diversity in the background of tumors and improving attention perceptual ability. A pixel-level illustration of this concept is shown in Fig.4. Since the hidden features are in accordance with the positions of pixels, the pixel level illustration

is comparable to the feature map of hidden layers.

The utility of performing local image translation can be considered as follows. Assume that a single tumor image has 12 patches, 1 of which include a piece of the tumor and 7 of which are blank. Without the additional translated normal images, the attention mechanism can only learn background information from up to 4 more patches. Doubling the number of useful patches around tumors helps the model to learn more variance from diverse yet informative backgrounds, enhancing generalization ability of attention.

Furthermore, the intrinsic property of medical images can help in the completion of the translation process. Since the backgrounds of most tumor images are identical to those of normal image, only the location of the tumor has a distinct distribution, so it’s important to introduce different backgrounds to assist in tumor detection.

4. Experiments

In this section, we will conduct thorough evaluations of our proposed REPLICa model on an open-source breast scan dataset, examining both image translation quality and object detection performance.

4.1. Experimental Settings

Digital Breast Tomosynthesis Dataset. We choose to use a publicly available dataset of breast cancer screening scans: the Digital Breast Tomosynthesis (BCS-DBT) dataset [5]. The BCS-DBT dataset comprises cancer cases that are normal, actionable, non biopsy-proven, and biopsy-proven. It contains 22032 breast tomosynthesis scans from 5060 individuals, with each scan containing up to 4 anatomical views and dozens of spatially-aligned slices in each view. Below are two examples of DBT images.

In our study, we randomly choose 5 slices from each view of a normal scan, therefore each normal scan will have up to 20 slices in our study. We preserve all 346 slices

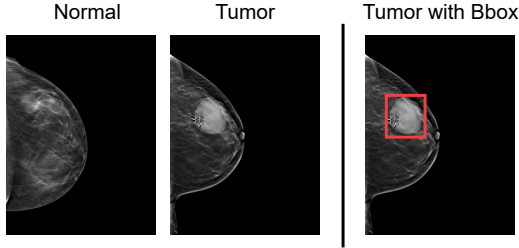


Figure 5. The examples of normal and tumor images from BCS-DBT. Red box denotes the bounding box of the tumor image.

with bounding boxes in both the training and validation sets for tumor scans that include both biopsy-proven benign and cancer tumors.

Following the dataset split information, we use 224 tumor slices with 271 bounding boxes as the training set, 75 tumor slices with 75 bounding boxes as the validation set and 136 tumor slices with 136 bounding boxes as the test set. We chose 3519 normal patients and the corresponding 70380 slices as the pool for pairing with tumor images, as shown in Tab.1.

Image Types	# of Image	# of Slices	# of Bboxes
Normal	3519	70380	N/A
Tumor	299	299	346

Table 1. The number of data from the DBT dataset that we used in our research.

Evaluation Metrics. We use a range of metrics to evaluate the quality of local image translation and the performance of object detection with attention on image feature patches. In the image reconstruction training process, we use the training set L_1 reconstruction loss being less than 0.01 to indicate overfitting.

We also use the AP (Average Precision) metrics for object detection as a quantitative study of our model. There are metrics relying on IoU (Intersection over Union) that describes the intersection of ground-truth bounding boxes and predicted bounding boxes from models. The IoU formula is known as

$$IoU(A, B) = \frac{|A \cap B|}{|A \cup B|}, \quad (7)$$

where A and B are ground-truth bounding boxes and predicted bounding boxes from models, respectively. $IoU(A, B) \in [0, 1]$.

In our study, we employ AP, AP50, AP75, APm, and API as analysis criteria, with AP50 serving as an indicator of model performance. Here, AP, AP50 and AP75 denote AP at IoU from 0.5 to 0.9 with step 0.05, IoU equals 0.5 and IoU equals 0.75, respectively. APm and API are for medium

objects with areas $\in [32^2, 96^2]$ and large objects with areas more than 96^2 .

The original Detectron2 framework [50] has random data augmentation that resizes images to 8 various shapes, some of which may be incompatible to our preset patch size, as the widths and heights of hidden feature maps should be an integer multiple of the width and heights of the preset patch. As a result, we remove the random data augmentation in the experiments. The entire Detectron2 framework will be indicated as ResNet50 with random augmentation, which will be introduced in the quantitative studies of 4.2.

We included the details of model implementation in the appendix for brevity.

4.2. Experimental Results

We provide both qualitative and quantitative results of our experiments. We characterize the quality of local image translation by examining three different physiological types of tumors to be translated into normal images, and evaluate tumor detection performance with our model.

Quantitative Results. We compare images as reconstructed by our local image translation module in 3.1 with the original tumor and paired normal images as shown in Fig.6. In our translation task, there are three types of tumors: tumors on the boundary, tumors inside the boundary, and small tumors. They correspond to the first, second, and third rows of the figure, respectively.

In the translation from one tumor image to the paired normal images, the translated normal images are consistent in both style and content, indicating that the translation was successful. This can be seen in the first row of the figure, with three implanted tumors that are in accordance with the equivalent normal image. In the second row of the figure, the translated normal image can have a texture and tissues that are consistent with the original texture and tissues. In the final row, a tumor of smaller size is also properly translated into the final output.

We also evaluated CycleGAN’s performance in terms of output image quality for both global and local image translation in the appendix.

Quantitative Evaluations. In the quantitative evaluations, we separated the local image translation in 3.1 and attention guided feature pyramid network in 3.2 as two components to the ResNet50 backbones. For local image translation, we generate three extra locally translated datasets using real cancerous images of the BCS-DBT dataset in 4.1. For the 47 tumor images that include multiple tumor annotations, we keep the first annotation as the location for translation. The statistics of dataset after generation is shown in Tab.2. We denote the model with realistic but fake additional images is called ResNet50 with local image translation (LIT).

We incorporate the attention-guided feature pyramid net-

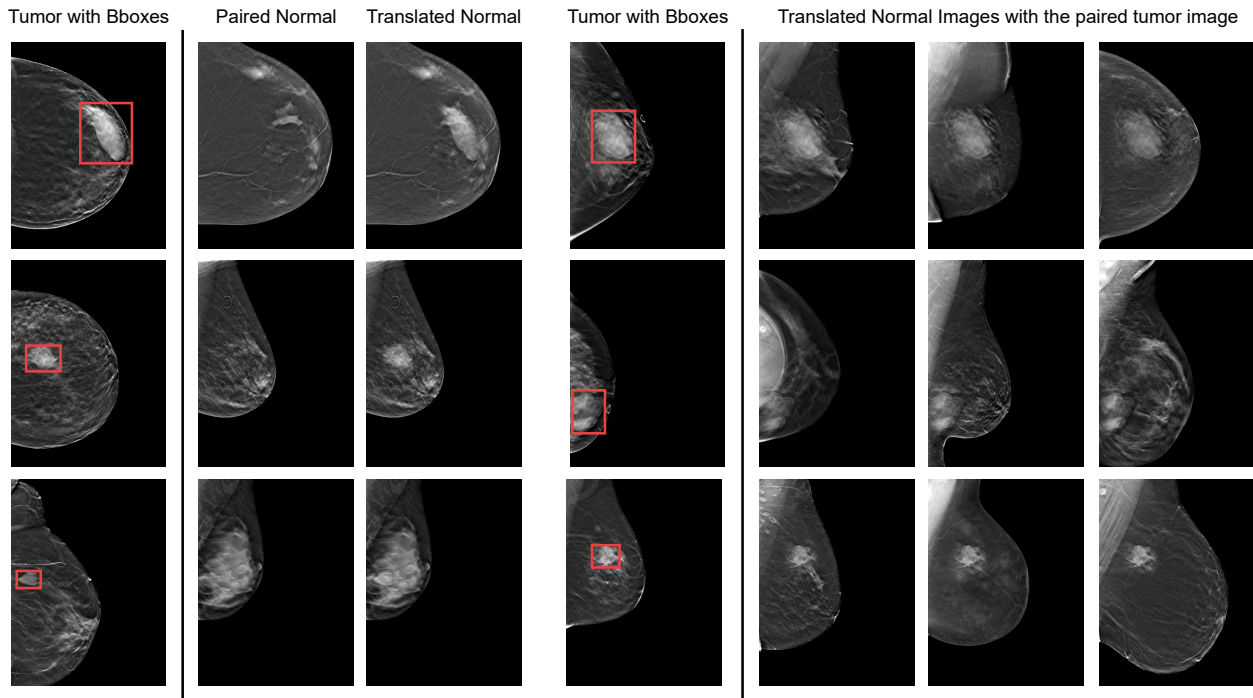


Figure 6. Examples of local image translation using convolutional autoencoder. The corresponding tumor for translation is shown by red boxes. The left side shows three tumor images as the source of translation, their paired normal images, and the normal images after translation. The right side shows three tumor images for translation and the translation results for three different paired normal images.

Image Types	# of Image	# of Slices	# of Bboxes
Tumor	299	299	346
Translated	665	665	665
Total	964	964	1011

Table 2. Dataset statistics for quantitative experiments. The dataset is a combination of tumor images from DBT dataset and locally translated normal data in 3.1.

work in 3.2 directly into the ResNet50 output without the use of additional translated images, which is named ViT-ResNet. In terms of the baseline ResNet50 model, we preserve both the version with and without Random Augmentation (RA). REPLICa has both local image translation module and the attention-guided feature pyramid network. In the quantitative evaluation method, we compare the performance of REPLICa with different backbones of Detectron2 [50], including the baseline ResNet50, ResNet50 with random augmentation, ResNet50 with our local image translation (LIT) in 3.1, ViT-ResNet and REPLICa, our final model.

As indicated in Tab.3, two modules of REPLICa can compensate for each other. As shown in the best results, when adding the local image translation module without using patch-based attention, the ResNet50 (LIT) performs better than ResNet50 (RA), showing the effectiveness of using

our translated images. When adding attention on image feature patches, the performance of ViT-ResNet50 improves significantly on the validation set, but remains lower than REPLICa. REPLICa outperforms other backbones in both the best and mean performance of the validation set.

When we switch to the mean results of the validation set, we notice some variations. While adding local image translation consistently improves performance of ResNet50 over ResNet50 (RA) on AP50, the performance of ViT-ResNet50 drops significantly, which is worse than ResNet50 (RA). This indicates to some extent that in the absence of sufficient data, attention mechanisms would show the instability of performance, partially demonstrated by the high variance of its AP50. Additionally, we found that adding locally translated photos can add variance to the detection of medium-sized tumors by ResNet50 (LIT). REPLICa mitigates this kind of variance while performing better than other backbones.

In terms of other criteria, we can see that ResNet50 (LIT) performs best in detecting large-sized tumors (API), demonstrating the efficiency of local image translation in assisting in the diagnosis of practically perceptible tumors. In addition, the ResNet50 (RA) performs best in AP, AP75 and APm, demonstrating the robustness of the whole convolutional structure under more strict detection criterion. REPLICa has the highest improvements in terms of AP50.

Model Backbone	AP at Validation Set (Best)					AP at Validation Set (Mean)					Variance	
	AP	AP50	AP75	APm	API	AP	AP50	AP75	APm	API	AP50	APm
ResNet50 (Baseline)	12.9	43.8	8.7	3.3	13.9	11.6	41.2	4.4	5.2	12.3	3.1	2.3
ResNet50 (RA)	15.0	46.6	4.9	16.5	14.6	15.2	44.4	7.1	14.4	15.4	2.5	4.8
ResNet50 (LIT)	14.9	47.8	6.4	20.3	13.8	14.4	45.9	4.8	13.8	15.7	2.2	33.8
ViT-ResNet50	13.1	49.6	2.3	3.7	14.1	12.4	43.2	3.7	6.7	13.0	16.5	14.6
REPLICA	15.7	50.4	4.7	8.5	16.5	13.4	49.0	3.3	6.3	14.4	1.7	6.8

Table 3. The performance of REPLICA and the models it compares. RA and LIT stand for Random Augmentation and Local Image Translation in 3.1, respectively. Each simulation was performed 5 times for computing the means and variances of criteria.

Aspect	Variant	AP (Best)	AP (Mean)	AP50 (Best)	AP50 (Mean)
REPLICA	N/A	15.7	13.4	50.4	49.0
Local Image Translation	Generative Image Translation	N/A	N/A	N/A	N/A
Local Image Translation	Translated Images Only	9.0 (-6.7)	8.2 (-5.2)	34.3 (-16.1)	31.2 (-17.8)
Attention Guided FPN	Feedforward Layers in ViT	13.5 (-2.2)	12.0 (-1.4)	41.1 (-9.3)	40.8 (-8.2)
Attention Guided FPN	Depth of Attention Layers	15.1 (-0.6)	12.1 (-1.3)	41.3 (-9.1)	39.5 (-9.5)

Table 4. Ablation studies of REPLICA. Local Image Translation and Attention Guided FPN are in the section of 3.1 and 3.2, respectively. In the experiment, each simulation was performed 5 times for computing the mean of AP and AP50.

4.3. Ablation Studies

We conduct ablation studies on REPLICA to validate each proposed modification in our approach, including modifications of translation method and attention, and present the results in Tab.4.

Generative Image Translation. We remove the progressive translation and change the translation model to CycleGAN [57]. The results are analyzed in the appendix, showing that CycleGAN can only change the styles and textures of healthy images and it is not compatible with tumor translation. We omit the simulation stage because there are no visible tumors in the outputs.

Translated Images Only To evaluate the effectiveness of our translated images, we study the model performance of REPLICA with our realistic but fake tumor images only. The performance of REPLICA in this dataset drops 31.9% but still has 34.3 for the best AP50, showing the effectiveness of local image translation and the necessity of combing them with real cancerous images.

Feedforward Layers in ViT We further study the effect of removing feedforward layers in ViT [16] by training REPLICA with one feedforward layer after an attention layer. This leads to a 18.5% decrease in the best AP50, indicating that by introducing non-linearity to the output of attention layers, feedforward layers are incapable of improving the attention mechanism in our scenario.

Depth of Attention Layers To value the effectiveness of our attention mechanism on image feature patches, we study the performance of REPLICA by default depth of attention layers in ViT. Adding additional one layer of attention leads to a 18.1% decrease in best AP50. Both of the

ablation studies of attention show the significance of the direct application of attention on image feature patches.

4.4. Limitations

A main limitation of our work is that our local image translation is specialized in translating medical images, which share similar textures, shapes and colors. It’s almost impossible to generalize our model to natural images [23] because they are highly diverse and distinct in both their foregrounds and backgrounds.

Moreover, our work rely on multiple times of training for a larger fake dataset, because we need to ensure the quality of translation by keeping a balanced number of healthy and tumor scans and using overfitting of the autoencoder.

Last, our attention-guided feature pyramid network is based on the standard object detection framework. According to the recent benchmarks of object detection, most SOTA models are fully transformer-based, including Soft Teacher + Swin-L [51] and DyHead [13]. We analyzed the incompatibility of these methods for breast tumor detection in 3.3, but comparisons with fully transformer-based methods are missing in our work.

5. Conclusion

We proposed the REPLICA model in this work to improve the performance of the object detection model in the context of breast tumor detection. As a novel pipeline for improving performance and stability of high-resolution breast tumor detection and achieve higher performance on existing backbones, REPLICA provides a new idea for related problems.

References

- [1] Saad Albawi, Tareq Abed Mohammed, and Saad Al-Zawi. Understanding of a convolutional neural network. In *2017 International Conference on Engineering and Technology (ICET)*, pages 1–6. Ieee, 2017. 3
- [2] Moab Arar, Yiftach Ginger, Dov Danon, Amit H Bermano, and Daniel Cohen-Or. Unsupervised multi-modal image registration via geometry preserving image-to-image translation. In *Proceedings of the IEEE/CVF conference on computer vision and pattern recognition*, pages 13410–13419, 2020. 2
- [3] Irwan Bello, Barret Zoph, Ashish Vaswani, Jonathon Shlens, and Quoc V Le. Attention augmented convolutional networks. In *Proceedings of the IEEE/CVF international conference on computer vision*, pages 3286–3295, 2019. 3
- [4] Puja Bharati and Ankita Pramanik. Deep learning techniques—r-cnn to mask r-cnn: A survey. In *Computational Intelligence in Pattern Recognition*, pages 657–668. Springer, 2020. 3
- [5] Mateusz Buda, Ashirbani Saha, Ruth Walsh, Sujata Ghate, Nianyi Li, Albert Święcicki, Joseph Y Lo, and Maciej A Mazurowski. A data set and deep learning algorithm for the detection of masses and architectural distortions in digital breast tomosynthesis images. *JAMA network open*, 4(8):e2119100–e2119100, 2021. 1, 2, 5
- [6] Zhaowei Cai, Quanfu Fan, Rogerio S Feris, and Nuno Vasconcelos. A unified multi-scale deep convolutional neural network for fast object detection. In *European conference on computer vision*, pages 354–370. Springer, 2016. 3
- [7] Nicolas Carion, Francisco Massa, Gabriel Synnaeve, Nicolas Usunier, Alexander Kirillov, and Sergey Zagoruyko. End-to-end object detection with transformers. In *European Conference on Computer Vision*, pages 213–229. Springer, 2020. 3
- [8] Kai Chen, Jiaqi Wang, Jiangmiao Pang, Yuhang Cao, Yu Xiong, Xiaoxiao Li, Shuyang Sun, Wansen Feng, Ziwei Liu, Jiarui Xu, Zheng Zhang, Dazhi Cheng, Chenchen Zhu, Tianheng Cheng, Qijie Zhao, Buyu Li, Xin Lu, Rui Zhu, Yue Wu, Jifeng Dai, Jingdong Wang, Jianping Shi, Wanli Ouyang, Chen Change Loy, and Dahua Lin. MMDetection: Open mmlab detection toolbox and benchmark. *arXiv preprint arXiv:1906.07155*, 2019. 3
- [9] Yunjey Choi, Minje Choi, Munyoung Kim, Jung-Woo Ha, Sunghun Kim, and Jaegul Choo. Stargan: Unified generative adversarial networks for multi-domain image-to-image translation. In *Proceedings of the IEEE conference on computer vision and pattern recognition*, pages 8789–8797, 2018. 2
- [10] Xiangxiang Chu, Zhi Tian, Yuqing Wang, Bo Zhang, Haibing Ren, Xiaolin Wei, Huaxia Xia, and Chunhua Shen. Twins: Revisiting the design of spatial attention in vision transformers. *arXiv preprint arXiv:2104.13840*, 1(2):3, 2021. 5
- [11] Marius Cordts, Mohamed Omran, Sebastian Ramos, Timo Scharwächter, Markus Enzweiler, Rodrigo Benenson, Uwe Franke, Stefan Roth, and Bernt Schiele. The cityscapes dataset. In *CVPR Workshop on The Future of Datasets in Vision*, 2015. 1
- [12] Tiago Cortinhal, Fatih Kurnaz, and Eren Erdal Aksoy. Semantics-aware multi-modal domain translation: From lidar point clouds to panoramic color images. In *Proceedings of the IEEE/CVF International Conference on Computer Vision*, pages 3032–3048, 2021. 2
- [13] Xiyang Dai, Yinpeng Chen, Jianwei Yang, Pengchuan Zhang, Lu Yuan, and Lei Zhang. Dynamic detr: End-to-end object detection with dynamic attention. In *Proceedings of the IEEE/CVF International Conference on Computer Vision*, pages 2988–2997, 2021. 1, 8
- [14] Jia Deng, Wei Dong, Richard Socher, Li-Jia Li, Kai Li, and Li Fei-Fei. Imagenet: A large-scale hierarchical image database. In *2009 IEEE Conference on Computer Vision and Pattern Recognition*, pages 248–255, 2009. 1
- [15] Jacob Devlin, Ming-Wei Chang, Kenton Lee, and Kristina Toutanova. Bert: Pre-training of deep bidirectional transformers for language understanding. *arXiv preprint arXiv:1810.04805*, 2018. 4
- [16] Alexey Dosovitskiy, Lucas Beyer, Alexander Kolesnikov, Dirk Weissenborn, Xiaohua Zhai, Thomas Unterthiner, Mostafa Dehghani, Matthias Minderer, Georg Heigold, Sylvain Gelly, et al. An image is worth 16x16 words: Transformers for image recognition at scale. *arXiv preprint arXiv:2010.11929*, 2020. 1, 3, 8
- [17] Zheng Ge, Songtao Liu, Feng Wang, Zeming Li, and Jian Sun. Yolox: Exceeding yolo series in 2021. *arXiv preprint arXiv:2107.08430*, 2021. 3
- [18] Ian Goodfellow, Jean Pouget-Abadie, Mehdi Mirza, Bing Xu, David Warde-Farley, Sherjil Ozair, Aaron Courville, and Yoshua Bengio. Generative adversarial nets. *Advances in neural information processing systems*, 27, 2014. 2
- [19] Yuchao Gu, Lijuan Wang, Ziqin Wang, Yun Liu, Ming-Ming Cheng, and Shao-Ping Lu. Pyramid constrained self-attention network for fast video salient object detection. In *Proceedings of the AAAI Conference on Artificial Intelligence*, volume 34, pages 10869–10876, 2020. 1
- [20] Kaiming He, Xiangyu Zhang, Shaoqing Ren, and Jian Sun. Deep residual learning for image recognition. In *Proceedings of the IEEE conference on computer vision and pattern recognition*, pages 770–778, 2016. 3
- [21] Han Hu, Zheng Zhang, Zhenda Xie, and Stephen Lin. Local relation networks for image recognition. In *Proceedings of the IEEE/CVF International Conference on Computer Vision*, pages 3464–3473, 2019. 1
- [22] Xun Huang, Ming-Yu Liu, Serge Belongie, and Jan Kautz. Multimodal unsupervised image-to-image translation. In *Proceedings of the European conference on computer vision (ECCV)*, pages 172–189, 2018. 2
- [23] Phillip Isola, Jun-Yan Zhu, Tinghui Zhou, and Alexei A Efros. Image-to-image translation with conditional adversarial networks. In *Proceedings of the IEEE conference on computer vision and pattern recognition*, pages 1125–1134, 2017. 2, 8
- [24] Diederik P Kingma and Max Welling. Auto-encoding variational bayes. *arXiv preprint arXiv:1312.6114*, 2013. 2

- [25] Diederik P Kingma and Max Welling. An introduction to variational autoencoders. *arXiv preprint arXiv:1906.02691*, 2019. **3**
- [26] Yehao Li, Ting Yao, Yingwei Pan, and Tao Mei. Contextual transformer networks for visual recognition. *arXiv preprint arXiv:2107.12292*, 2021. **3**
- [27] Hezheng Lin, Xing Cheng, Xiangyu Wu, Fan Yang, Dong Shen, Zhongyuan Wang, Qing Song, and Wei Yuan. Cat: Cross attention in vision transformer. *arXiv preprint arXiv:2106.05786*, 2021. **5**
- [28] Tsung-Yi Lin, Piotr Dollár, Ross Girshick, Kaiming He, Bharath Hariharan, and Serge Belongie. Feature pyramid networks for object detection. In *Proceedings of the IEEE conference on computer vision and pattern recognition*, pages 2117–2125, 2017. **2, 4**
- [29] Tsung-Yi Lin, Michael Maire, Serge Belongie, James Hays, Pietro Perona, Deva Ramanan, Piotr Dollár, and C Lawrence Zitnick. Microsoft coco: Common objects in context. In *European conference on computer vision*, pages 740–755. Springer, 2014. **1**
- [30] Alexander H Liu, Yen-Cheng Liu, Yu-Ying Yeh, and Yu-Chiang Frank Wang. A unified feature disentangler for multi-domain image translation and manipulation. *arXiv preprint arXiv:1809.01361*, 2018. **2**
- [31] Ming-Yu Liu, Thomas Breuel, and Jan Kautz. Unsupervised image-to-image translation networks. In *Advances in neural information processing systems*, pages 700–708, 2017. **2**
- [32] Nian Liu, Ni Zhang, Kaiyuan Wan, Ling Shao, and Junwei Han. Visual saliency transformer. In *Proceedings of the IEEE/CVF International Conference on Computer Vision*, pages 4722–4732, 2021. **3**
- [33] Yahui Liu, Marco De Nadai, Jian Yao, Nicu Sebe, Bruno Lepri, and Xavier Alameda-Pineda. Gmm-unit: Unsupervised multi-domain and multi-modal image-to-image translation via attribute gaussian mixture modeling. *arXiv preprint arXiv:2003.06788*, 2020. **2**
- [34] Ze Liu, Yutong Lin, Yue Cao, Han Hu, Yixuan Wei, Zheng Zhang, Stephen Lin, and Baining Guo. Swin transformer: Hierarchical vision transformer using shifted windows. *arXiv preprint arXiv:2103.14030*, 2021. **1**
- [35] Ziwei Liu, Ping Luo, Xiaogang Wang, and Xiaoou Tang. Deep learning face attributes in the wild. In *Proceedings of International Conference on Computer Vision (ICCV)*, December 2015. **1**
- [36] Scott Mayer McKinney, Marcin Sieniek, Varun Godbole, Jonathan Godwin, Natasha Antropova, Hutan Ashrafian, Trevor Back, Mary Chesus, Greg S Corrado, Ara Darzi, et al. International evaluation of an ai system for breast cancer screening. *Nature*, 577(7788):89–94, 2020. **1**
- [37] Ajeet Ram Pathak, Manjusha Pandey, and Siddharth Rautaray. Application of deep learning for object detection. *Procedia computer science*, 132:1706–1717, 2018. **1**
- [38] Prajit Ramachandran, Niki Parmar, Ashish Vaswani, Irwan Bello, Anselm Levskaya, and Jonathon Shlens. Stand-alone self-attention in vision models. *arXiv preprint arXiv:1906.05909*, 2019. **1**
- [39] Joseph Redmon, Santosh Divvala, Ross Girshick, and Ali Farhadi. You only look once: Unified, real-time object detection. In *Proceedings of the IEEE conference on computer vision and pattern recognition*, pages 779–788, 2016. **3**
- [40] Shaoqing Ren, Kaiming He, Ross Girshick, and Jian Sun. Faster r-cnn: Towards real-time object detection with region proposal networks. *Advances in neural information processing systems*, 28:91–99, 2015. **2, 3, 4**
- [41] Elad Richardson, Yuval Alaluf, Or Patashnik, Yotam Nitzan, Yaniv Azar, Stav Shapiro, and Daniel Cohen-Or. Encoding in style: a stylegan encoder for image-to-image translation. In *Proceedings of the IEEE/CVF Conference on Computer Vision and Pattern Recognition*, pages 2287–2296, 2021. **2**
- [42] Yujun Shen, Jinjin Gu, Xiaoou Tang, and Bolei Zhou. Interpreting the latent space of gans for semantic face editing. In *Proceedings of the IEEE/CVF Conference on Computer Vision and Pattern Recognition*, pages 9243–9252, 2020. **2**
- [43] Aravind Srinivas, Tsung-Yi Lin, Niki Parmar, Jonathon Shlens, Pieter Abbeel, and Ashish Vaswani. Bottleneck transformers for visual recognition. In *Proceedings of the IEEE/CVF Conference on Computer Vision and Pattern Recognition (CVPR)*, pages 16519–16529, June 2021. **3**
- [44] Mingxing Tan, Ruoming Pang, and Quoc V. Le. Efficientdet: Scalable and efficient object detection. In *Proceedings of the IEEE/CVF Conference on Computer Vision and Pattern Recognition (CVPR)*, June 2020. **3**
- [45] Hugo Touvron, Matthieu Cord, Matthijs Douze, Francisco Massa, Alexandre Sablayrolles, and Hervé Jégou. Training data-efficient image transformers & distillation through attention. In *International Conference on Machine Learning*, pages 10347–10357. PMLR, 2021. **5**
- [46] Ashish Vaswani, Prajit Ramachandran, Aravind Srinivas, Niki Parmar, Blake Hechtman, and Jonathon Shlens. Scaling local self-attention for parameter efficient visual backbones. In *Proceedings of the IEEE/CVF Conference on Computer Vision and Pattern Recognition*, pages 12894–12904, 2021. **3**
- [47] Ashish Vaswani, Noam Shazeer, Niki Parmar, Jakob Uszkoreit, Llion Jones, Aidan N Gomez, Łukasz Kaiser, and Illia Polosukhin. Attention is all you need. In *Advances in neural information processing systems*, pages 5998–6008, 2017. **1, 3, 5**
- [48] Pei Wang, Yijun Li, Krishna Kumar Singh, Jingwan Lu, and Nuno Vasconcelos. Imagine: Image synthesis by image-guided model inversion. In *Proceedings of the IEEE/CVF Conference on Computer Vision and Pattern Recognition*, pages 3681–3690, 2021. **2**
- [49] Wenhai Wang, Enze Xie, Xiang Li, Deng-Ping Fan, Kaitao Song, Ding Liang, Tong Lu, Ping Luo, and Ling Shao. Pyramid vision transformer: A versatile backbone for dense prediction without convolutions. *arXiv preprint arXiv:2102.12122*, 2021. **5**
- [50] Yuxin Wu, Alexander Kirillov, Francisco Massa, Wan-Yen Lo, and Ross Girshick. Detectron2. <https://github.com/facebookresearch/detectron2>, 2019. **3, 6, 7**
- [51] Mengde Xu, Zheng Zhang, Han Hu, Jianfeng Wang, Lijuan Wang, Fangyun Wei, Xiang Bai, and Zicheng Liu. End-to-

- end semi-supervised object detection with soft teacher. *arXiv preprint arXiv:2106.09018*, 2021. 8
- [52] Junbo Yin, Jianbing Shen, Xin Gao, David Crandall, and Ruigang Yang. Graph neural network and spatiotemporal transformer attention for 3d video object detection from point clouds. *IEEE Transactions on Pattern Analysis and Machine Intelligence*, 2021. 1
- [53] Xiaoming Yu, Yuanqi Chen, Thomas Li, Shan Liu, and Ge Li. Multi-mapping image-to-image translation via learning disentanglement. *arXiv preprint arXiv:1909.07877*, 2019. 2
- [54] Fangneng Zhan, Yingchen Yu, Kaiwen Cui, Gongjie Zhang, Shijian Lu, Jianxiong Pan, Changgong Zhang, Feiying Ma, Xuansong Xie, and Chunyan Miao. Unbalanced feature transport for exemplar-based image translation. In *Proceedings of the IEEE/CVF Conference on Computer Vision and Pattern Recognition*, pages 15028–15038, 2021. 2
- [55] Zhong-Qiu Zhao, Peng Zheng, Shou-Tao Xu, and Xindong Wu. Object detection with deep learning: A review. *IEEE Transactions on Neural Networks and Learning Systems*, 30(11):3212–3232, 2019. 3
- [56] Zhaohui Zheng, Ping Wang, Wei Liu, Jinze Li, Rongguang Ye, and Dongwei Ren. Distance-iou loss: Faster and better learning for bounding box regression. In *Proceedings of the AAAI Conference on Artificial Intelligence*, volume 34, pages 12993–13000, 2020. 3
- [57] Jun-Yan Zhu, Taesung Park, Phillip Isola, and Alexei A Efros. Unpaired image-to-image translation using cycle-consistent adversarial networks. In *Proceedings of the IEEE international conference on computer vision*, pages 2223–2232, 2017. 2, 8
- [58] Jun-Yan Zhu, Richard Zhang, Deepak Pathak, Trevor Darrell, Alexei A Efros, Oliver Wang, and Eli Shechtman. Multi-modal image-to-image translation by enforcing bi-cycle consistency. In *Advances in neural information processing systems*, pages 465–476, 2017. 2